Article

In Silico Infrared Spectroscopy as a Benchmark for Identifying Seized Samples Suspected of Being *N*-Ethylpentylone

Caio H. P. Rodrigues [1], Ricardo de O. Mascarenhas [2] and Aline T. Bruni [1,*]

[1] Departamento de Química e Instituto Nacional de Ciência e Tecnologia Forense (INCT Forense), Faculdade de Filosofia, Ciências e Letras de Ribeirão Preto, Universidade de São Paulo, Avenida Bandeirantes, 3900, Vila Monte Alegre, Ribeirão Preto 14040-901, SP, Brazil
[2] Polícia Federal, Setor Técnico-Científico, Rua Profa. Sandália Monzon, 210, Santa Cândida, Curitiba 82640-040, PR, Brazil
* Correspondence: aline.bruni@usp.br

Abstract: New psychoactive substances (NPSs) have concerned authorities worldwide, and monitoring them has become increasingly complex. In addition to the frequent emergence of new chemical structures, the composition of adulterants has changed rapidly. Reliable reference data on NPS are not always available, and identifying them has become an operational problem. In this study, we evaluated the infrared spectral data of 68 seized samples suspected of containing a synthetic cathinone (*N*-ethylpentylone). We used quantum chemistry tools to simulate infrared spectra as a benchmark and obtained infrared spectra for different cathinones, structurally analogous amphetamines, and possible adulterants. We employed these in silico data to construct different chemometric models and investigated the internal and external validation and classification requirements of the models. We applied the best models to predict the classification of the experimental data, which showed that the seized samples did not have a well-defined profile. Infrared spectra alone did not allow *N*-ethylpentylone to be distinguished from other substances. This study enabled us to evaluate whether experimental, in silico, and applied statistical techniques help to promote forensic analysis for decision-making. The seized samples required in-depth treatment and evaluation so that they could be correctly analyzed for forensic purposes.

Keywords: *N*-ethylpentylone; DFT; PLS-DA

1. Introduction

New psychoactive substances (NPSs) are compounds that are not controlled by the 1961 (Single Convention on Narcotic Drugs) or the 1971 (Convention on Psychotropic Substances) conventions in their respective pure forms or in mixtures. Because there is no indication of control, they have become a threat to public health, in many countries [1–3]. Some NPSs have been known for over 30 years, so the term "new" does not necessarily refer to novel drugs but rather to drugs that have recently become a threat to public health [3,4]. NPSs include different compounds, and synthetic cathinones (SC) are the second-most detected. Between 2009 and 2021, the United Nations Office on Drugs and Crime (UNODC) reported 1127 NPSs and identified 17.8% (201) of them as SC [1,3]. In Brazil, *N*-ethylpentylone is the most seized SC, and therefore, its correct identification is important for law enforcement agencies.

The rapid emergence of these different structures demands techniques that provide information faster and nondestructively, to aid decision-making. Spectroscopy has proven suitable for detecting and identifying NPSs [5]. Spectroscopic techniques (transmission, absorption, or reflection) are based on the interaction of matter with radiant energy [6]. Among spectroscopic techniques, near and middle infrared (NIR and MIR, respectively) spectroscopy stands out: NIR and MIR are easy to implement and have short response times [7–9]. NIR and MIR are based on the alteration of the dipole moment of molecules

(overtones), which allows their vibrations to be analyzed [10,11]. Compared with other techniques, NIR and MIR provide results rapidly, are nondestructive, and require low-cost instrumentation. In addition, sample preparation is simple, and these techniques can be applied to analyze samples in the liquid, semisolid, and solid states [12,13].

In the forensic domain, the Scientific Working Group for the Analysis of Seized Drugs (SWGDRUG) recommends that these techniques be classified in the highest category (category A) because they are selective and provide structural information [14,15]. Because of this selectivity, these techniques have been miniaturized, which has made them portable and allowed them to be directly applied to places of interest [16–21]. There are other, more-robust methods that can provide structural information on isomers, such as NMR [22–26], GC-MS [27–29], and LC-MS [30–32].

Chemometrics is a mathematical approach that can complement and amplify spectroscopic interpretation given that it can add information for decision-making [33]. Together, chemometric and spectroscopic techniques improve our understanding of instrumental data and can be applied in different areas of forensic science [34]. Chemometric studies have been carried out on blood traces [35], urine traces for sex discrimination [36], soils [37], biological traces [38], textile fibers [39], and vehicle bumper fragments [40], among others [41–45]. The combination of chemometric and spectroscopic methods applied to experimental analyses of classic illicit drugs is already being widely used [7,35,37,38,43,46].

Nevertheless, identifying NPSs remains challenging. In the case of cathinones, homologous amphetamines can impair correct recognition because of structural similarities [47–49]. More costly techniques are usually applied to resolve this situation [50–53]. According to the UNODC, 23 signatory countries have generic legislation for controlling NPSs, but not all of them distinguish between amphetamines and cathinones. Another point that deserves attention is interferents, which make spectroscopic characterization even more complex. Interferents and drugs can have similar appearances (in the case of diluents) and physiological properties (in the case of adulterants), which can make investigations difficult and pose unpredictable health risks [54–56].

Here, we investigated the combination of computational and chemometric methods to evaluate Fourier-transform infrared (FTIR) spectroscopy experimental data. We used only computational methods to obtain benchmarks for detecting *N*-ethylpentylone in seized samples. The idea was to demonstrate that in silico methods can offer a protocol for decision-making and an alternative for assessing unknown samples for which no analytical standard was available or accessible.

2. Materials and Methods
2.1. Part I—Experimental Analyses

Sixty-eight samples suspected of containing *N*-ethylpentylone (Figure 1), a synthetic cathinone, were seized in Brazil and analyzed in investigations coordinated by the Federal Police (PF) in 2017.
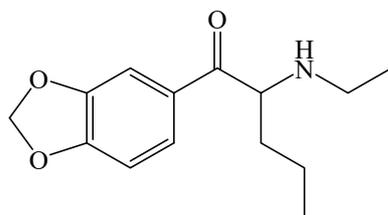
Figure 1. Structure of the molecule known as *N*-ethylpentylone or Ephylone, IUPAC nomenclature 1-(2H-1,3-benzodioxol-5-yl)-2-(ethylamino)pentan-1-one, CAS 727641-67-0 with molecular weight of 249.31 (base) or 285.77 (HCl salt form).

The samples were ground and homogenized before being inserted into the attenuated total reflectance (ATR) accessory. The FTIR spectra were recorded on a Thermo Fisher Scientific Nicolet 380 spectrometer (Madison, WI, USA) equipped with a Smart Orbit

(Madison, WI, USA) single-ATR reflection diamond crystal. However, the ATR accessory is known to distort the spectrum—bands with higher wave numbers are "undersized", and bands with lower wave numbers are "oversized" [8]. Thus, ATR was corrected by using OMNIC software version 7.2a, also by Thermo Fisher Scientific (Thermo Electron Corporation, now Thermo Fisher Scientific, Madison, WI, USA). To reduce noise, the average spectra of the samples obtained after 32 readings were evaluated.

Gaussian distribution was employed to ensure that the experimental data and the simulated data had the same dimension. The results ranged from 4000 to 525 cm^{-1}; the resolution was 2 cm^{-1}. The generated data were organized in a spreadsheet (Excel, Microsoft Office 365, Redmond, Washington, DC, USA), and their resolution was resized to be consistent with the routine analysis (4 cm^{-1}). In addition, these data later underwent statistical analysis and prediction. The variables were not pretreated.

2.2. Part II—Computational Analyses

Different NPSs were simulated, namely *N*-ethylpentylone; *N*-ethylpentylanoamine (an amphetamine homologous to *N*-ethylpentylone); 21 amphetamines (Figure 2A); 21 cathinones homologous to amphetamines (Figure 2B), available in Table S1 of Supplementary Materials; and 12 other possible interferents (creatine, phenacetin, lidocaine, LSD, paracetamol, procaine, psilocin, 25H-NBOMe, benzocaine, caffeine, metoclopramide, and theobromine).

(A)

(B)
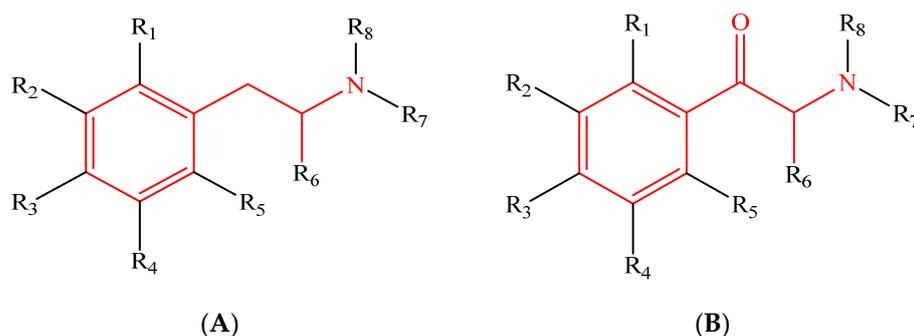
Figure 2. Schematic representation of the molecular structures of the class of (**A**) amphetamines and (**B**) cathinones.

On the basis of previous results [57], the functional DFT B3LYP [58] with the TZVP base [59–61], implemented in ORCA software version 4.2.1 [62], was selected for conducting this stage of the work and describing the structures. This combination was used to optimize the structures and to obtain the frequencies. For the analyses, chloroform was considered an implicit solvent; the conductor-like polarizable continuum model (CPCM) [63,64] was employed. A correction (scaling factor) of the theoretical data compared with the experimental data was performed for the selected method; the scaling factor was 0.9650 [65].

After the calculation, the data referring to the spectra in the infrared region were organized in a spreadsheet (Excel, Microsoft Office 365). As in the case of the experimental data, Gaussian distribution was applied to fit the simulated data from 4000 to 525 cm^{-1}, with a resolution of 4 cm^{-1}. This approach allowed the spectra to be combined, to obtain a set of mixtures that will serve as input for creating statistical models.

2.3. Part III—Statistical Analyses

Statistical analyses and/or data validation were used in each previous step. This approach ensured the practical construction of forecast models that were later applied to the samples of interest. Thus, a similarity analysis was carried out by employing a heat map as a tool to understand the possible divergences between the nature of the compounds present in the seized samples [66].

2.3.1. Experimental Data

The 68 samples that were experimentally analyzed by ATR-FTIR contained heterogeneous errors that were not constant, because the synthesis of the compounds was not standardized. Because of the complexity of these samples, evaluation started with a simple exploratory analysis. In this step, the intensities at each wavelength were evaluated by using Pearson's correlation coefficient (Equation (1)):

$$r = \frac{\sum_i (x_i - \bar{x}) \cdot (y_i - \bar{y})}{\sqrt{\sum_i (x_i - \bar{x})^2 \cdot \sum_i (y_i - \bar{y})^2}} \tag{1}$$

This coefficient allows the strength of the two variables to be quantified. If $r = 1$, the relationship is positive and the variables are directly proportional. If $r = -1$, the association indicates that the variables are inversely proportional [66]. The responses obtained through this correlation were analyzed by employing a heat map and a histogram to quantify the occurrences of correlation between the spectra and by using separatrices (quartiles). These analyses were performed in a spreadsheet (Excel, Microsoft Office 365).

2.3.2. Models with the Computational Data

For the computational analysis step, the obtained data were used to formulate models to investigate whether *N*-ethylpentylone was present in the seized samples. The partial least squares discriminant analysis (PLS-DA) technique was employed to develop these models.

PLS-DA performs classification through multivariate regression, in which the dependent variable consists of a vector that divides the samples into target classes (numerically identified as +1 and −1). PLS-DA decomposes the data matrix X, which contains n samples and m variables (matrix $X_{(n,m)}$). In this case, the independent variables are the computationally obtained data corresponding to the vibrations in the infrared region. Decomposition of the data matrix gives rise to new axes (latent variables) that gather information from the original variables [5,33]. This technique consists of a multivariate classification analysis implemented in Pirouette software version 4.5 (Infometrix, Bothell, Washington, DC, USA).

Leave-one-out (LOO) cross-validation was applied in this stage of model construction [67,68]. LOO cross-validation consists of removing a sample and then reassessing the model to predict the sample that was removed. This occurs systematically until all the samples have been subjected to the process. The parameters used to evaluate the PLS-DA results are Q^2, internal correlation coefficient of the cross-validation model (Equation (2)); R^2, correlation coefficient for calibration (Equation (3)); RMSEV, root mean square error validation (Equation (4)); and RMSEC, root mean square error calibration (Equation (5)):

$$Q^2 = 1 - \frac{\sum_i (y_i - y_{cv})^2}{\sum_i \left(y_i - \bar{y}_i\right)^2} \tag{2}$$

$$R^2 = 1 - \frac{\sum_i (y_i - y_{cal})^2}{\sum_{i=1} \left(y_i - \bar{y}_i\right)} \tag{3}$$

$$RMSEV = \sqrt{\frac{\sum_{i=1}^{I} \left(y_i - \hat{y}_i\right)^2}{I}} \tag{4}$$

$$RMSEC = \sqrt{\frac{\sum_{i=1}^{I} \left(y_i - \hat{y}_i\right)^2}{v}} \tag{5}$$

These parameters are evaluated independently and through the relations $R^2 > Q^2$ and RMSEC < RMSEV [69]. More specifically, the high value of R^2 represents low data variability, resulting in low root mean square error calibration (RMSEC) because few data are unexplained by the model.

After the models were constructed by using the computationally obtained spectra, the datasets were evaluated by employing the methodology of internal and external validation, which started with leave-N-out (LNO) cross-validation, where N varied from 1 to 10 for all the models. The mean (Q^2_{LNO}, N = 10), the variation between LOO and LNO, and the standard deviation were evaluated. For the model to be robust, the difference between Q^2_{LNO} and Q^2_{LOO} must be minimal [70].

For external validation, the computationally obtained datasets were divided into submodels by applying the Kennard–Stone algorithm [71], available in Dataset Division 1.2 software (Jadavpur, Kolkata, West Bengal, India). This method calculates the Euclidean distances from the dataset, and the two most-distant samples, most dispersed in space, are selected to group the others. We defined that a subgroup would gather 75% of the original data and another 25%, so the algorithm generates training and test sets. This approach assesses the prediction ability of the models, as well as their stability and robustness [72,73].

2.3.3. Assessing the Predictive Capacity of Models

The models were analyzed by using the computationally obtained data (validated internally and externally) to evaluate performance, sensitivity, specificity, precision, and accuracy. Experimental infrared data from monographs available in the SWGDRUG library version 2.1 (available at https://www.swgdrug.org/ir.htm, JCAMP Format, accessed on 21 March 2022) were used. The monographs of 20 amphetamines and 20 cathinones (available in Table S2 of Supplementary Materials) were selected because these compounds are analogous to the compound of interest in the study. All these new data were submitted to the same procedure of resizing the wavelengths to adjust the matrix for the chemometric processes. The models were used to evaluate not only the NPSs but also 20 adulterants with similar structures (available in Table S3 of Supplementary Materials).

In this evaluation, the values related to each class, either + 1 or −1, were employed as cutoff limits. The samples that showed a positive and a negative value were considered to belong entirely to the class indicated as +1 and −1, respectively. The cutoff limit was used because it allowed the responses to be evaluated through figures of merit (FOMs).

This way, these known spectra obtained from the SWGDRUG libraries were submitted to the prediction model. Thus, the answers with (i) false-positive (FP), samples of class α erroneously assigned to class β; (ii) false-negative (FN), samples of class β wrongly assigned to class α; (iii) true-negative (TN), samples of class α correctly assigned to class α; and (iv) true-positive (TP), samples of class β correctly assigned to class β were inserted [56]. With this information, the parameters' sensitivity (Equation (6)), specificity (Equation (7)), precision (Equation (8)), and accuracy (Equation (9)) were employed to assess the robustness of the created models [74–76].

$$\frac{\textbf{TP}}{\textbf{TP} + \textbf{FN}} \tag{6}$$

$$\frac{\textbf{TN}}{\textbf{TN} + \textbf{FP}} \tag{7}$$

$$\frac{\textbf{TP}}{\textbf{TP} + \textbf{FP}} \tag{8}$$

$$\frac{\textbf{TN} + \textbf{TP}}{\textbf{TN} + \textbf{FP} + \textbf{TP} + \textbf{FN}} \tag{9}$$

This analysis enables the qualitative methods to be validated and ensures better reliability for the statistical procedure applied to the samples of interest. Thus, this evaluation

more safely indicates the probability that a new sample (characteristics resembling the characteristics used to create the model) belongs or not to classes [5].

2.3.4. Predicting the Samples of Interest

After the models were validated and their precision was evaluated, the experimental data of the 68 samples seized by the Federal Police and suspected of being *N*-ethylpentylone were used. Figure 3 summarizes the entire experimental procedure used here.
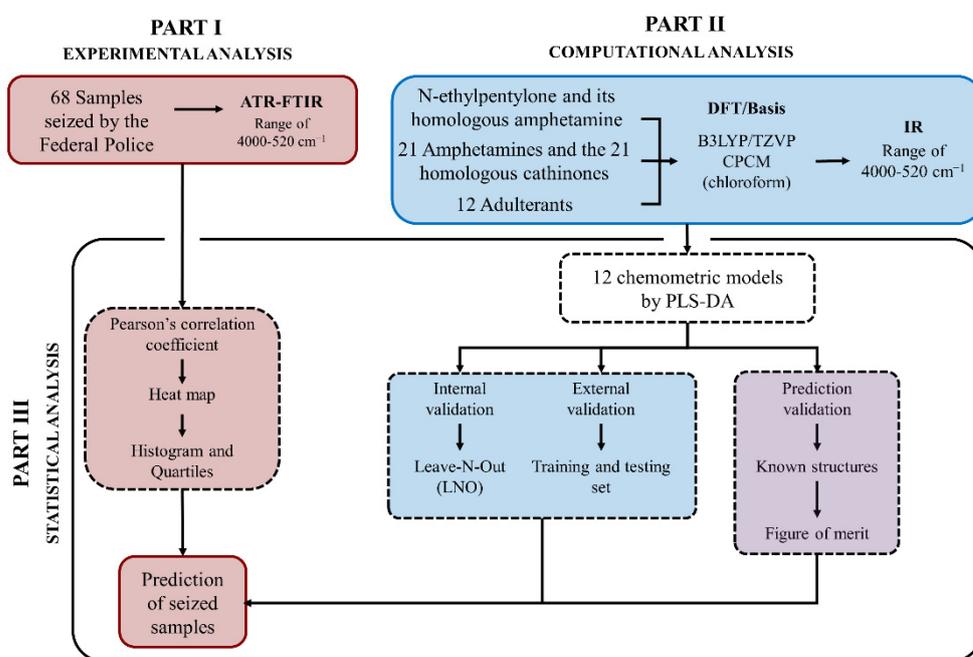
Figure 3. Schematic summary of the procedures used in this work: red for experimental data; blue for computational data; and purple for experimental data obtained from the SWGDRUG library of monographs.

3. Results

3.1. Part I—Experimental Analyses

The analyzed samples had been seized by the Brazilian Federal Police in 2017. They were initially identified as possibly being the synthetic cathinone known as *N*-ethylpentylone because their spectral profile resembled the spectral profile of *N*-ethylpentylone in the monograph available in the SWGDRUG library (Figure 4) [77]. The seized samples initially had labels on their packages indicating that they were food for dogs and cats (Figure 5), with different delivery destinations.

We analyzed the seized samples by spectroscopy in the infrared region without applying any analytical preparation to obtain the spectra. We ground, homogenized, and inserted the samples into the ATR accessory. We collected spectra from 4000 to 525 cm^{-1}, with spectral resolutions of 4 cm^{-1}. To reduce noise, in this analysis, we used the average spectra obtained after 32 readings, a standard protocol used by the Brazilian Federal Police.

We did not use the 400–525 cm^{-1} range, because the diamond employed in the equipment absorbs in this region. We analyzed 68 samples and obtained the average spectrum of each of them. Figure 6 groups the superposition of these average spectra obtained by the described methodology. We will use the nomenclature indicated in this figure throughout sample processing.
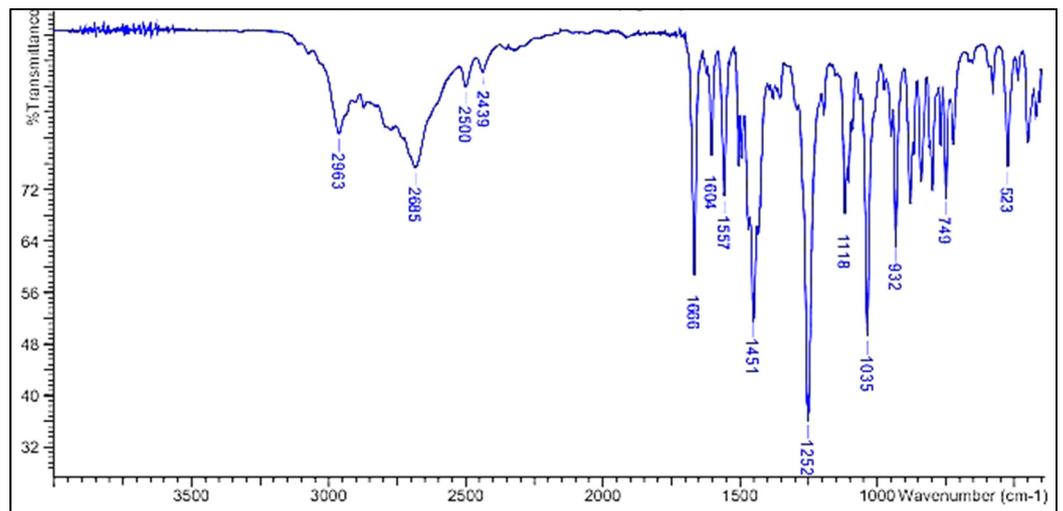
Figure 4. Infrared spectrum for *N*-ethylpentylone deposited in the SWGDRUG library of monographs [77].

(**a**)	(**b**)	(**c**)

Figure 5. Seizure of samples suspected of containing *N*-ethylpentylone: (**a**) Federal Police seized the samples packaged as dog food and cat food; (**b**) samples inside the packages; (**c**) crystals suspected of being an NPS.

-2160	-2163	-2167	-2168	-2174	-2176	-2177	-2178	-2180	-2181A	-2181B	-2184A	-2184B	-2221
2177	2225	2228	2229	2230	2231	2232	2233	2234	2235	2236A	2236B	2237	2238A
2238B	2239	2240	2265	2266	2267	2269	2269B	2269C	2269D	2269E	2270	2271	2273
2274	2275	2276A	2276B	2277B	2279	2280	2282	2284A	2284B	2288	2289	2293	2293B
-2297	-2300	-2357	-2358	-2372	-2374	-2376	-2414	-2417	-2426	-2429A	-2429B		
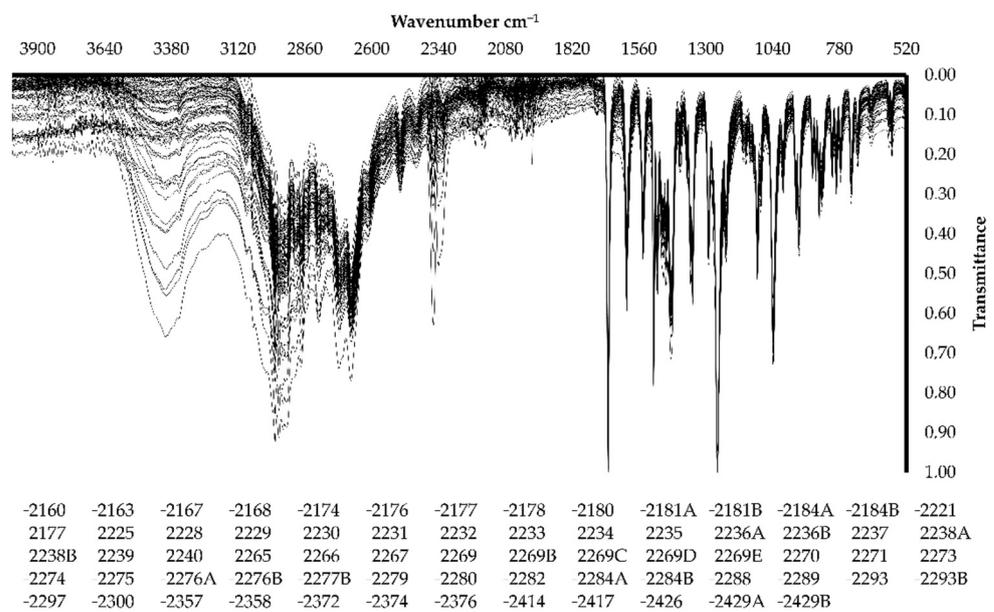
Figure 6. Overlay of mean spectra obtained by the FTIR-ATR of the samples suspected of containing *N*-ethylpentylone.

We observed that the samples had similar spectra. We used descriptive statistics, Pearson's correlation coefficient (Equation (1)), to assess the initial similarity of these data [78].

Additionally, we employed the peaks between 800 cm^{-1} and 1700 cm^{-1} and between 2788 cm^{-1} and 3480 cm^{-1} for this evaluation because the spectra had these regions in common. We removed these regions from the data because they could introduce a doubtful aspect to the responses if we were to use them [79]. Figure 7 illustrates the relationships between the experimentally evaluated samples (available in Table S4 of Supplementary Materials).
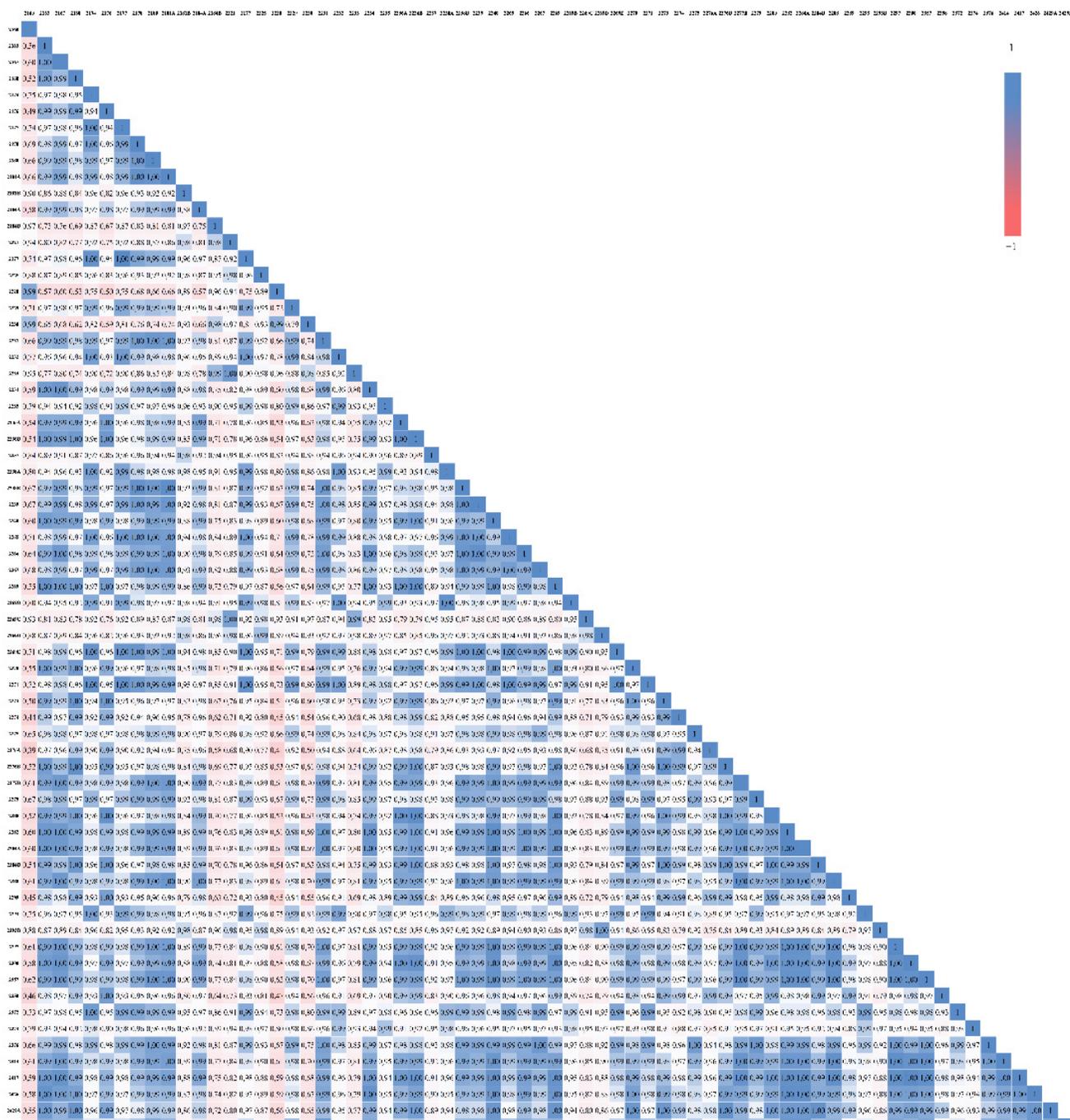
Figure 7. Heat map obtained by Pearson's correlation coefficient for samples suspected of being *N*-ethylpentylone.

Figure 7 shows very similar samples and divergent samples. No comparison was less than zero, indicating that all the samples were correlated. More objectively, Figure 8 summarizes these comparisons through a histogram. The red line represents the cumulative variation of these occurrences for each segment of the evaluated spectral range. We observed that most samples were around similarity (0.5–0.6), and a few samples, less than 20%, had high likeness.
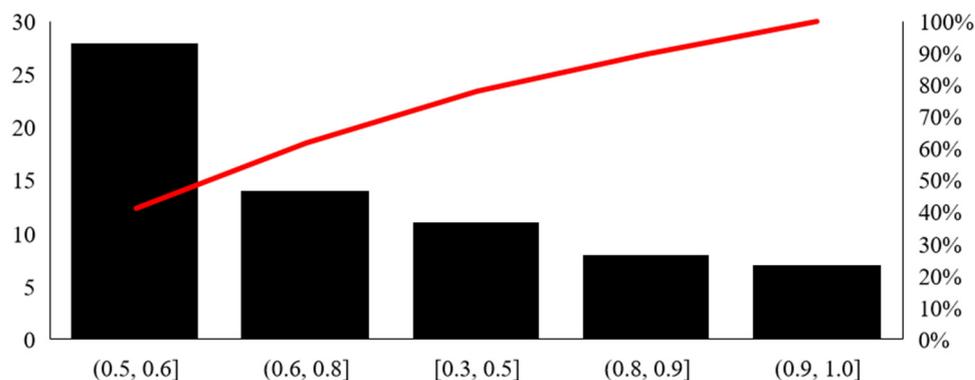
Figure 8. Histogram with the distribution of the occurrences for comparison between the experimental spectral data.

This analysis showed that the experimental spectra of the samples suspected of containing *N*-ethylpentylone and the spectrum available for *N*-ethylpentylone in the SWGDRUG library of monographs had some similarity. However, we did not evaluate the samples for possible interferences or the presence of other compounds that may have the same response. Figure 9 indicates the correlation between the spectra of the 68 samples seized by the Federal Police and the reference spectrum for *N*-ethylpentylone deposited in the SWGDRUG library of monographs.
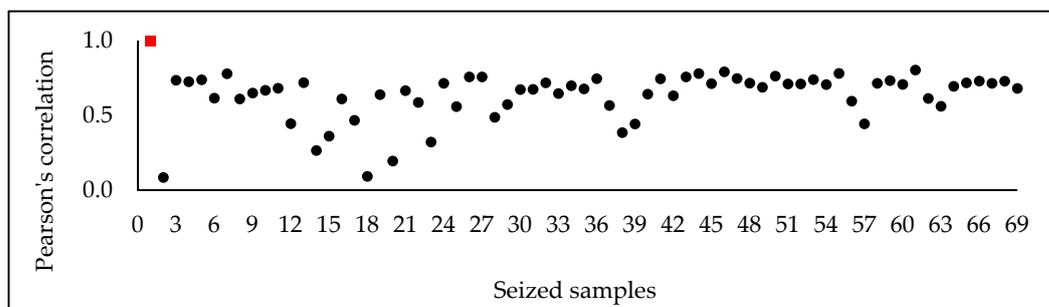
Figure 9. Pearson's correlation applied to compare the seized samples—circles in black—and the spectrum in the infrared region deposited in the SWGDRUG library of monographs—square in red—used as a reference for *N*-ethylpentylone by forensic entities.

On the basis of Figure 9, the values ranged from 0.09 to 0.80. More specifically, about 83% (57 of 68) of the samples had values between 0.20 and 0.75. This wide range indicated uncertainties and the need for a detailed analysis of which samples were similar or different [80]. We better explored this range (Figure 9) on the basis of the data presented in Table 1. These results gather the numerical values for the quartiles and allow the dataset to be analyzed more accurately.

Table 1. Maximum, minimum, and quartile values for the experimental data compared with the spectrum available on the SWGDRUG platform.

Descriptive Statistical Used	Quartile Value	Description
Minimum	0.0863	Lowest value within the set
Maximum	0.8041	Highest value within the set
1st quartile	0.5944	25% of the data are found below this value
2nd quartile	0.6856	Median or 50% of the data are found below this value
3rd quartile	0.7304	75% of the data are found below this value
4th quartile	0.8041	Maximum value or 100% of the data are found below this value

From the analysis summarized in Table 1, 50% of the dataset correlated up to 0.6856, and 75% of the evaluated spectra correlated up to 0.7304. Given the need for analytical standards, we used a spectral survey through computational analysis to identify which spectra could contain *N*-ethylpentylone.

3.2. Part II—Computational Analyses

We simulated 21 amphetamines, 21 cathinones [45], and 12 adulterants. We obtained all these results by using chloroform as the implicit solvent and the functional DFT B3LYP with the TZVP base. All the obtained data resulted in structures with positive vibrational frequencies, which ensured that the structures were in a structural conformation of minimum energy [81].

Because the theoretical spectra use harmonic approximations and do not consider some anharmonic effects in the calculations, the wavelengths obtained in the simulation were shifted [82]. To correct these responses, we used the scaling factor 0.9650, available at NIST (National Institute of Standards and Technology) [65].

We applied the Gaussian distribution [83] to the obtained frequency data. This approach fit the simulated data in the experimental data dimension. For this, we used the wavelengths from 520 to 1700, from 2788 to 3156 cm^{-1}, and from 3316 to 3480 cm^{-1} with resolution resembling the resolution of the experimental data, totaling 431 wavelengths.

Additionally, we combined the frequency for each pair of simulated compounds to acquire the resulting spectrum of the mixture. The proposal was to simulate the addition of adulterants to the spectra of the different NPSs studied here. This combination allowed us to construct data matrixes for use during chemometric analyses. Table 2 shows the resulting mixtures.

Table 2. Composition of the chemometric models obtained from the combination or not of computationally obtained spectra.

Combination	Group 1	Group 2	Samples
1	Individual amphetamines	Individual cathinones	42
2	Amphetamines with adulterants	Cathinones with adulterants	504
3	Amphetamines with *N*-ethylpentylone	Cathinones with *N*-ethylpentylone	42
4	Amphetamines with *N*-ethylpentylanoamine	Cathinones with *N*-ethylpentylanoamine	42
5	Individual amphetamines	Adulterants with *N*-ethylpentylone	24
6	Individual adulterants	Adulterants with *N*-ethylpentylanoamine	24
7	Individual amphetamines	Amphetamines with *N*-ethylpentylone	42
8	Individual amphetamines	Amphetamines with *N*-ethylpentylanoamine	42
9	Individual cathinones	Cathinones with *N*-ethylpentylone	42
10	Individual cathinones	Cathinones with *N*-ethylpentylanoamine	42
11	Individual amphetamines with *N*-ethylpentylone	Individual cathinones and with *N*-ethylpentylone	84
12	Individual amphetamines with *N*-ethylpentylanoamine	Individual cathinones and with *N*-ethylpentylanoamine	84

3.3. Part III—Statistical Analysis

We used the combinations shown in Table 2 to create the PLS-DA models. More specifically, the data matrixes contained 431 variable wave numbers, referring to the computationally obtained spectroscopic results. We grouped the values obtained for each of the models in Table 3.

Table 3. Parameters of the developed PLS-DA models.

Models	Principal Components	%Information	R^2	Q^2	$\Delta(R^2-Q^2)$	RMSEC	RMSEV
M1	3	71.8776	0.9253	0.8936	0.0317	0.2840	0.3278
M2	4	71.9650	0.7763	0.7593	0.0170	0.4748	0.4908
M3	3	94.3680	0.9008	0.8181	0.0827	0.3268	0.4324
M4	3	93.3712	0.9624	0.9132	0.0492	0.2041	0.2978
M5	6	67.9705	0.7322	0.0189	0.7133	0.5977	1.1309
M6	7	77.2237	0.7264	0.2588	0.4676	0.6219	0.9778
M7	3	85.0025	0.9249	0.8003	0.1246	0.2846	0.4488
M8	6	92.5215	0.9204	0.6357	0.2848	0.3047	0.6119
M9	6	94.6613	0.8709	0.7627	0.1082	0.3881	0.4948
M10	3	88.5391	0.8647	0.8292	0.0355	0.3820	0.4149
M11	3	78.9113	0.7660	0.7252	0.0408	0.4936	0.5278
M12	3	83.4734	0.8444	0.8243	0.0201	0.4019	0.4201

On the basis of the results in Table 3, the parameters varied for each model. The principal components varied from 3 to 7, with accumulated information from 67.9705% (M5) to 94.6613% (M9). The correlation coefficient for calibration (R^2) ranged from 0.7264 (M6) to 0.9624 (M4). We obeyed the other parameters according to the relationship exposed in Equations (2) to (5). Furthermore, the difference between the values of R^2 and Q^2 varied between 0.0170 (M2) and 0.7133 (M5) [84,85].

We applied the leave-n-out (LNO) test to assess the stability of the cross-validation coefficient (Q^2) of the models. In addition, we grouped the results on Q^2_{LNO} variations in Table 4.

Table 4. Cross-validation test result of models M1 to M12.

Model	Q^2_{LOO} (N=1)	Q^2_{LNO} (Average, N = 10)	$\|\Delta(Q^2_{LOO}-Q^2_{LNO})\|$	S (St. Desv.)	Maximum Variation
M1	0.8936	0.8934	0.0002	0.0092	$Q^2_{L6O} = 0.9055$
M2	0.7593	0.7982	0.0389	0.0140	$Q^2_{L6O} = 0.8071$
M3	0.8181	0.8024	0.0157	0.0258	$Q^2_{L5O} = 0.8271$
M4	0.9132	0.9035	0.0097	0.0170	$Q^2_{L6O} = 0.9197$
M5	0.0189	0.0712	0.0523	0.0539	$Q^2_{L6O} = 0.1671$
M6	0.2588	0.2063	0.0525	0.0506	$Q^2_{L6O} = 0.2938$
M7	0.8003	0.8079	0.0076	0.0224	$Q^2_{L2O} = 0.8462$
M8	0.6357	0.6175	0.0182	0.0344	$Q^2_{L6O} = 0.6901$
M9	0.7627	0.7543	0.0084	0.0107	$Q^2_{L4O} = 0.7689$
M10	0.8292	0.8315	0.0023	0.0161	$Q^2_{L6O} = 0.8491$
M11	0.7252	0.7294	0.0042	0.0126	$Q^2_{L8O} = 0.7485$
M12	0.8243	0.8245	0.0002	0.0109	$Q^2_{L7O} = 0.8380$

We observed that the responses for Q^2_{LNO} in the models ranged from 0.0712 (M5) to 0.9035 (M4), with standard deviations of 0.0506 and 0.0170, respectively. LOO and LNO differed from 0.0002 (M1 and M12) to 0.0525 (M6) units. This information allowed us to observe the stability of the models given that a high standard deviation and an extensive range of values between Q^2_{LOO} and Q^2_{LNO} indicate internal problems in the validated dataset. Thus, we conducted external validation to evaluate the robustness of the models and how adjusted they were. Table 5 gathers the resulting parameters for this validation.

Table 5. Parameters obtained with external validation by using the Kennard–Stone method for dividing datasets.

Model	Training Set	Test Set	SEP	PRESS	R^2	% Hit
M1	31	11	0.4076	1.8277	0.9196	100.0%
M2	378	126	0.5591	39.3867	0.7083	90.5%
M3	30	12	0.9103	9.9434	0.1739	66.7%
M4	30	12	1.1510	15.8975	0.0020	50.0%
M5	18	6	1.52×10^5	1.39×10^{11}	0.0307	66.7%
M6	18	6	1.17×10^5	8.16×10^{10}	0.0008	66.7%
M7	30	12	0.8640	8.9586	0.4143	75.0%
M8	30	12	0.7638	6.9998	0.4580	91.7%
M9	30	12	0.3862	1.7901	0.8510	91.7%
M10	30	12	0.7670	7.0597	0.4784	91.7%
M11	62	22	0.8914	17.4794	0.2064	72.7%
M12	62	22	0.9912	21.6154	0.0635	54.5%

The submodels obtained by the Kennard–Stone method provided the parameters described in Table 5. The R^2 values ranged from 0.9196 (M1) to 0.0008 (M6), indicating that the models with the lowest correlation were very well adjusted to the dataset. Moreover, the SEP and PRESS values also provided information about the modeling error: the higher the value, the greater the residual error.

We validated the predictions on the basis of the consistency between the evaluated and validated (both internally and externally) models and the dataset obtained by the simulation. For this approach, we used experimental spectra in the infrared region of known structures available on the SWGDRUG platform. The procedure consisted of predicting the classification of amphetamines (20), cathinones (20), and adulterants (20) known in the models. We used the figures of merit to evaluate these responses. With the responses obtained by applying the logical tests, we received information about the sensitivity, specificity, precision, and accuracy of the model. Table 6 gathers the results for the logical tests applied to the predictions and robustness percentages.

Table 6. Responses of the figures of merit and the robustness of the models obtained by using computationally obtained data.

Model	FP	TN	FN	TP	Sensitivity	Specificity	Precision	Accuracy
M1	0	20	3	17	85.0%	100.0%	100.0%	92.5%
M2	2	18	3	17	85.0%	90.0%	89.5%	87.5%
M3	0	20	3	17	85.0%	100.0%	100.0%	92.5%
M4	2	18	2	18	90.0%	90.0%	90.0%	90.0%
M5	17	3	0	20	100.0%	15.0%	54.1%	57.5%
M6	17	3	0	20	100.0%	15.0%	54.1%	57.5%
M7	2	18	1	19	95.0%	90.0%	90.5%	92.5%
M8	9	11	7	13	65.0%	55.0%	59.1%	60.0%
M9	13	7	11	9	45.0%	35.0%	40.9%	40.0%
M10	20	0	17	3	15.0%	0.0%	13.0%	7.5%
M11	0	20	8	12	60.0%	100.0%	100.0%	80.0%
M12	1	19	2	18	90.0%	95.0%	94.7%	92.5%

We used the parameters indicated by Equations (6) to (9) to evaluate these predictions. We observed that models M1, M2, M3, M4, M7, and M12 presented values above 85% for sensitivity, specificity, precision, and accuracy. The other models either proved to be very specific and not very sensitive or very sensitive and not very specific. Furthermore, these different models did not have adequate accuracy.

We included *N*-ethylpentylone in the group of cathinones used to verify the predictive capacity. Because *N*-ethylpentylone is the structure of interest in this work, we included

its spectrum, made available by the SWGDRUG library of monographs, in this dataset. Thus, we included this molecule in the group used to evaluate the predictive capacity of the models by using known NPS structures. Table 7 combines the values and classes predicted for *N*-ethylpentylone by the models.

Table 7. Prediction value for the experimental spectrum of *N*-ethylpentylone in the different models developed in this work and the class indicated as correct.

Model	Forecast Value for *N*-ethylpentylone (c15)	Expected Classes
M1	−0.46	Individual cathinones
M2	−0.18	Cathinones with adulterants
M3	−0.71	Cathinone with *N*-ethylpentylone
M4	−1.27	Cathinone with *N*-ethylpentylanoamine
M5	−2.06	Adulterants with *N*-ethylpentylone
M6	−1.64	Adulterants with *N*-ethylpentylanoamine
M7	−1.38	Amphetamines mixed with *N*-ethylpentylone
M8	−0.58	Amphetamines mixed with *N*-ethylpentylanoamine
M9	0.13	Individual cathinones
M10	0.27	Individual cathinones
M11	0.13	Individual and mixed amphetamines with *N*-ethylpentylone
M12	−0.70	Individual cathinones and mixed with *N*-ethylpentylanoamine

Only two models (M6 and M8) were not able to predict the spectrum of *N*-ethylpentylone itself or a homologous cathinone correctly. The other models predicted the correct class.

From the same ideal of evaluating the predictive capacity of the models, we used the experimental data available in the SWGDRUG library of monographs for adulterants. We expected that the models would not indicate the presence of NPSs, because the data concerned only adulterants. However, the models were not able to predict the 20 spectra of the adulterants in the infrared region, as illustrated in Figure 10.
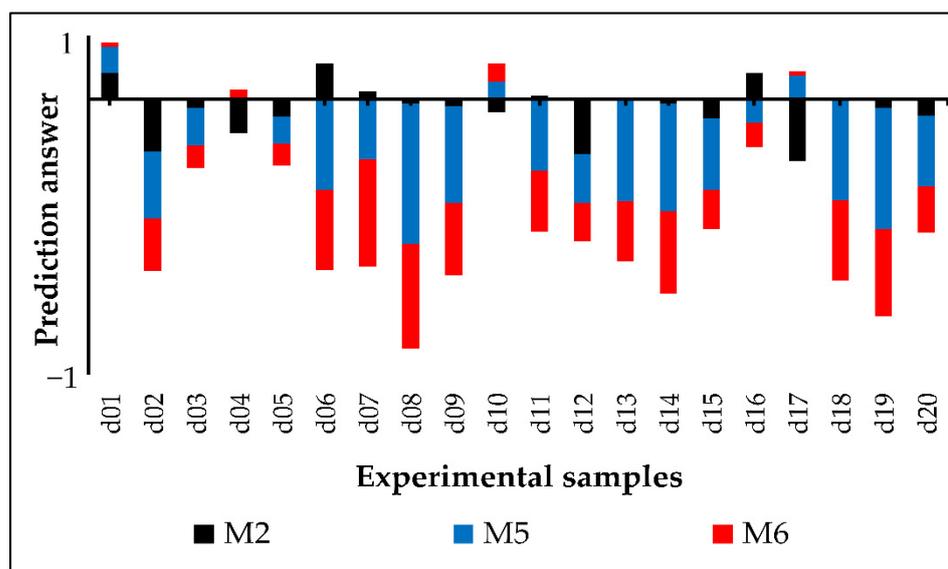
Figure 10. Prediction of the spectra in the infrared region of 20 adulterants obtained from the SWGDRUG library of monographs. The black bars group together the ratings for the model that contained the 21 amphetamines (+1) and cathinones (−1) mixed with adulterants (model M2). The blue bars gather the predictions by using the models containing only the pure adulterants (+1) and combine them with *N*-ethylpentylone (−1) (model M5). Finally, the red bars illustrate the predictions by using the model that contained the pure adulterants (+1) and their mixture with the amphetamine homologous to *N*-ethylpentylone (model M6).

For the most part, we observed that the classification of adulterants was erroneously predictive. The models indicated that they belonged to classes that contained some NPSs and not just individual adulterants. We observed that models M5 and M6 correctly predicted only samples d01, d10, and d17. Model M1 (in black) foresaw five possible adulterants (d01, d06, d07, d11, and d16) in the class of amphetamines mixed with adulterants (positive values in this model) and 15 possible adulterants in the class of cathinones with adulterants (negative values in this model).

Finally, Table 8 summarizes all the information obtained during the performed validations and evaluations. The symbol ✓ indicates that the modeling or validation parameters or the figures of merit were obeyed. If the parameters were not reached, they are shown with the symbol x.

Table 8. Summary of evaluations carried out on the basis of the modeling parameters, validations, and figures of merit for the developed models.

Model	PLS-DA Models	Cross-Validation	External Validation	Figure of Merit
M1	✓	✓	✓	✓
M2	✓	✓	✓	✓
M3	✓	✓	x	✓
M4	✓	✓	x	✓
M5	x	x	x	x
M6	x	x	x	x
M7	x	✓	x	✓
M8	x	x	x	x
M9	x	✓	✓	x
M10	✓	✓	x	x
M11	✓	x	x	x
M12	✓	✓	x	✓

Cells in red represent models that did not meet the minimum assessment requirements; those in green indicate the models that satisfactorily met the evaluated parameters.

Models M1 and M2 presented the best responses for all the analyses. We understand that external validation is a crucial step in evaluating the dataset. Therefore, we disregarded models M3 and M4 in the subsequent analyses.

3.4. Forecasting Seized Samples by PLS-DA

On the basis of the modeling carried out with the computationally obtained data (Table 3), the internal (Table 4) and external (Table 5) validations, and the analysis of figures of merit (Table 6), we submitted the experimental data originating from the arrests of the Federal Police Brazilian to the forecast. In the first stage of this work, we analyzed 68 samples suspected of containing the *N*-ethylpentylone in their composition (Figure 6). Thus, we used models with adequate sensitivity, specificity, precision, and accuracy for the prediction, to reduce the rate of false positives or false negatives, as indicated in Table 8.

We performed the prediction of these samples, and interpretation of the results followed the principle. The more positive or negative, the greater the correspondence with the class indicated in that model. In Figure 11, we summarized the ranking results for the two best models (numerical values in Table S5 of Supplementary Materials).

The prediction provided by these two models indicated the presence of some structure resembling amphetamines in the seized samples. In Figure 11a, model M1 predicted that 32 of the 68 samples were individual amphetamines and that the others were individual cathinones (36 of 68). As expected, model M2 indicated that all the samples belonged to classes containing amphetamines with adulterants and not cathinones.

We used the percentile function to return the k-th values in a range. As described in Table 9, we explored the percentages from 10% to 100%.

(a)

(b)
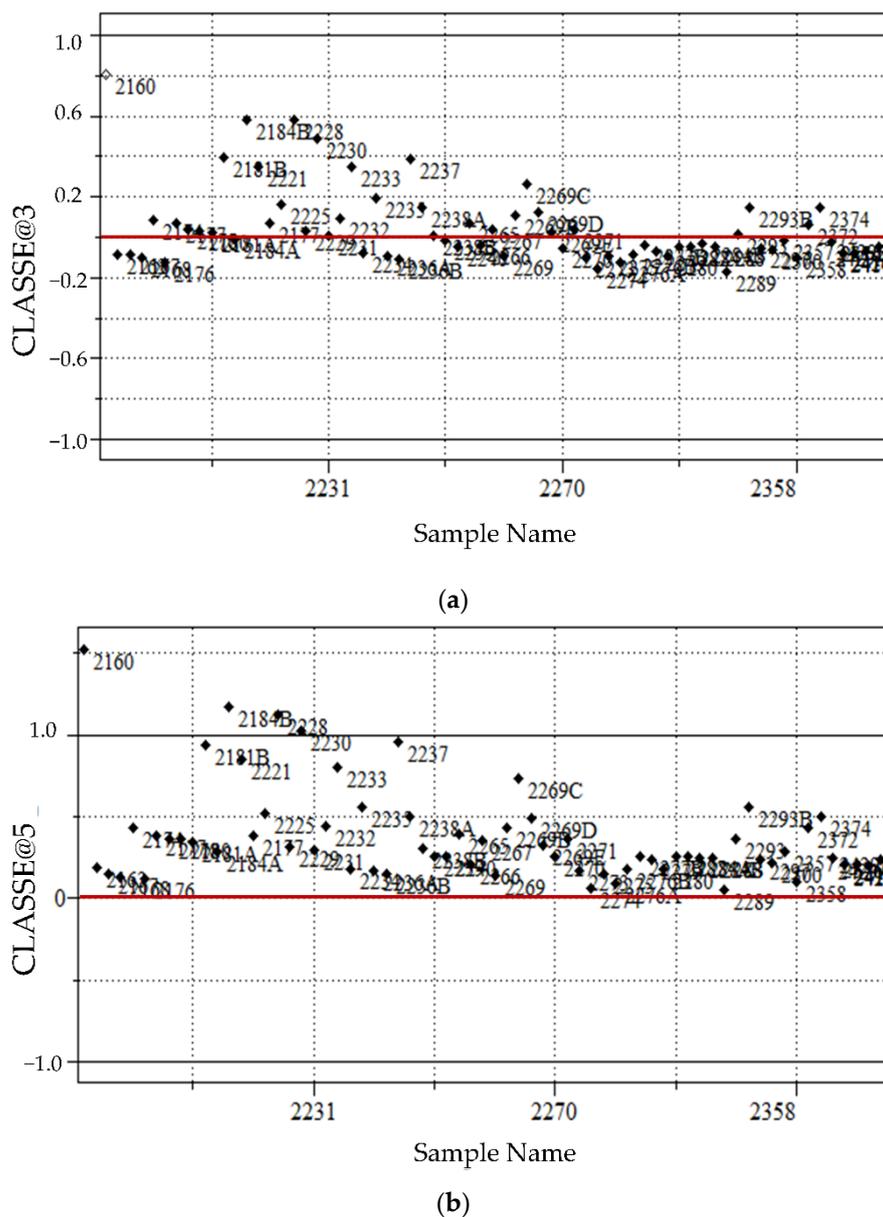
Figure 11. Prediction of samples suspected of being *N*-ethylpentylone in the models: (**a**) M1—individual amphetamines and cathinones; and (**b**) M2—amphetamines and cathinones with adulterants.

Table 9. Summary of percentiles for the classification of seized samples suspected of being *N*-ethylpentylone in models M1 and M2.

Percentile	M1	M2	Description
10%	−0.10	0.15	10% of the results are below this value.
30%	−0.06	0.22	30% of the results are below this value.
50%	−0.01	0.28	50% of the results are below this value.
60%	0.02	0.35	60% of the results are below this value.
70%	0.07	0.38	70% of the results are below this value.
80%	0.14	0.49	80% of the results are below this value.
90%	0.35	0.82	90% of the results are below this value.
100%	0.80	1.52	All responses are below this value.

On the basis of the responses summarized in Table 9, we observed that model M1 classified 50% of the seized samples as cathinones (negative values) and the remaining

samples as amphetamines (positive values). We observed dispersed results regarding model M2, indicating that the samples may have various constitutions.

4. Discussion

When we analyzed the experimental data by comparing Figures 4 and 6, we observed that the samples had similar profiles. However, in Figure 7, we observed that some samples were not correlated, indicating that the compositions were not homogeneous. Figure 8 reinforced this observation, as most samples showed similarity of less than 0.6. Only less than 20% of the samples showed similarity higher than 0.8. Interpreting spectra in the infrared region is not trivial and cannot be done by direct comparison (match), because the two spectra might be considerably similar while the compounds have different compositions. Indeed, infrared spectroscopy indicates bands of chemical groups, which may belong to different molecules [10]. These similarity metrics do not discriminate against structural differences in that there may be instrumental problems or sample impurities [86].

Given that there is no quality control for drugs, interferents may have a similar infrared profile, possibly generating uncertainties in the analyses. These interfering compounds can be (i) adulterants, compounds added to mimic some of the effects expected for these drugs, or (ii) diluents, compounds that do not produce psychoactive effects but can increase the bulk [87,88].

To reproduce this condition, we also computed the spectra of possible adulterants, 21 amphetamines, and 21 other cathinones, *N*-ethylpentylone, and its similar amphetamine. We used these data to prepare the training sets that were the basis of the models described in Table 2.

Table 3 indicated that the relations $R^2 > Q^2$ and RMSEC < RMSEV were respected in all cases. Moreover, the difference between R^2 and Q^2 suggests that the possibility of the models being overfitted to the data will be minimum, so this value should be the minimum possible [85]. Thus, the cutoff criterion used for this evaluation corresponded to values lower than 0.1 [84].

Tables 4 and 5 refer to internal (crossed) and external validations (using the Kennard–Stone algorithm). We observed that the models that contained only the adulterants could not specifically indicate the compounds. The responses in Figure 11 reinforced this observation and suggested that the spectroscopic characteristics of the adulterants were diffuse, so this group of compounds could be more significant or would need to be mixed. This group did not provide cohesion for the adequate modeling of the classes. Furthermore, the responses indicated that other studies to evaluate mixtures by computational means are possible.

Table 6 allowed us to evaluate the predictive capacity of the models, as a validation of the prediction, through figures of merit. With this approach, we were able to observe the sensitivity, specificity, prediction, and accuracy of detecting samples resembling the study system. By using spectral data from known samples, which are already employed as references in several forensic laboratories, we validated the predictive capacity of the models developed with computationally obtained data. In this evaluation with real experimental data, models M1, M2, M3, M4, M7, and M12 provided the best rates of correct classification. Table 7, which shows the predictions for the *N*-ethylpentylone spectrum available in the SWGDRUG library of monographs, reinforced this observation.

Table 8 allowed us to analyze all the responses together and to make more-assertive decisions when choosing the best model. Thus, we conducted the other analyses by using only models M1 and M2, which presented sensitivity, specificity, and accuracy values above 85%. In addition, these models were under the other evaluated parameters.

Finally, we predicted samples suspected of being *N*-ethylpentylone, seized by the Brazilian Federal Police. The responses showed that the presence of amphetamines could be identified in most samples. In model M1, 47.1% and 52.9% of the samples belonged to the class of pure amphetamines and cathinones, respectively. When the presence of possible

adulterants was considered, as in the case of model M2, all the samples were classified as belonging to the class of amphetamines with adulterants.

Given that the infrared spectroscopy technique allows functional groups and some intra- and intermolecular interactions to be analyzed, the technique was not enough to identify the single structures of amphetamines or cathinones in the samples. In models M1 and M2, most samples presented nominal values very close to the limit, around zero. Therefore, the identity of the compound as amphetamine or cathinone must be confirmed by ancillary techniques.

Different studies have applied spectroscopy in the infrared region to identify illicit drugs in seizures or to aid in harm reduction. Dixon et al. evaluated three techniques (FTIR, ^{1}H NMR, and GC-MS) for obtaining information on the drug composition of seized samples [89]. The authors concluded that analyzing response acquisition time and precision is important. If the objective involves quick responses, FTIR is the most appropriate technique. If accurate analysis is targeted, GC-MS is chosen. GC-MS is widely accepted as the gold standard for monitoring drug supply [90,91]. However, the method cannot provide timely information for consumers to make a decision or for police to seize samples. Thus, other techniques, such as infrared spectroscopy with Fourier-transform, ultraviolet-visible spectroscopy, or Raman spectroscopy, would be necessary. In all cases, two (or more) analytical methods are needed to validate the presence or absence of a substance [14,90]. Wallace et al. proposed implementing multiple techniques to indicate the composition of drugs consumed in the context of a party [92]. For infrared analysis, they evaluated fentanyl-like drugs and compared them with the SWGDRUG library. The evaluations were limited to the available database. Green et al. also used different techniques, including FTIR, to analyze fentanyl drugs obtained from seizures. However, one of the main criticisms of using this technique is the need for updated sample libraries [93].

According to these results, although SWGDRUG classifies spectroscopy in the infrared region as Category A for pure or high-purity samples [14], specific conditions still need to be discussed. Issues related to spectroscopic analysis can occur because of (i) the resolution, (ii) linearity corrections, (iii) the absence of analytical standards for NPSs, (iv) the type of mathematical corrections used to collect interferograms, and (v) the amount of the sample [7,86], which justifies the use of interpretation through chemometric methods in conjunction with spectroscopic analysis [7].

Developing chemical drug profiles through modeling allows (i) the more assertive comparison of samples to be made, (ii) the geographic origin to be identified, (iii) drug trafficking and distribution to be tracked, (iv) the chemical reagents used in production to be assessed, and (v) interferences (diluents and/or adulterants) to be identified [94]. In addition to that, the structural alterations of psychoactive compounds are frequently found in the context of NPSs. Clandestine laboratories have no control, insecurity factors, and possible cross-contamination [4].

The results obtained here are essential because seized NPSs are becoming increasingly diverse and contain countless possible adulterants. However, as much as there is an information gap that needs to be filled for fast decision-making, a new discussion on spectroscopy in the infrared region is needed. This technique has been recently consolidated because of its instrumental facility and potential for providing faster responses than other methods. However, differentiating between similar structures or characterizing contaminated samples must be considered.

The information obtained and analyzed here needs to be combined into a larger context of forensic intelligence, where the data are put into perspective [95–99]. This procedure allows the problem to be understood with alternative information from different methodologies to solve crimes and to support decision-making [100–102].

5. Conclusions

We applied spectroscopy in the infrared region to obtain prompt information in the repressive context and for harm reduction. The proposed computational approach

can identify amphetamines and/or cathinones in seized samples. The combination of computational simulation and statistical methods adequately sets a benchmark for new psychoactive substances. PLS-DA can predict the unknown samples in the modeled classes. However, infrared spectroscopy cannot differentiate between *N*-ethylpentylone and its homologous amphetamine. The reason for this behavior must be assessed so that the real influence of adulterants on the spectra can be determined. A more detailed study of the interferents may also be required. Other techniques, such as GC-MS, must provide more-assertive identification in a forensic laboratory. Literature shows similar conclusions [89–93]. Nevertheless, this study can give presumptive information and be a first step toward using computer simulation to compose benchmarks for in situ comparison. A more robust dataset can aid in decision-making in a multidisciplinary and integrated context of NPS forensics.

Creating a comprehensive dataset to follow international surveillance trends can be meaningful. The methodology studied in this work provides essential and adaptable information to identify new substances or harmful contaminants. The main advantage is that these benchmarks dismiss the need for laboratory supplies and regulatory authorizations. Using computational standards associated with chemometrics can be helpful for law enforcement and human rights in that these standards reduce the time needed for conducting the experimental tests.

Author Contributions: C.H.P.R.: conceptualization, methodology, validation, formal analysis, investigation, data curation, writing—original draft, visualization; R.d.O.M.: methodology, formal analysis, data curation, writing—original draft; A.T.B.: conceptualization, writing—original draft, supervision, project administration, funding acquisition. All authors have read and agreed to the published version of the manuscript.

References

1. Chou, H.-H.; Hsieh, C.-H.; Chaou, C.-H.; Chen, C.-K.; Yen, T.-H.; Liao, S.-C.; Seak, C.-J.; Chen, H.-Y. Synthetic Cathinone Poisoning from Ingestion of Drug-Laced "Instant Coffee Packets" in Taiwan. *Hum. Exp. Toxicol.* **2021**, *40*, 1403–1412. [CrossRef] [PubMed]
2. United Nations Office on Drugs and Crime GLOBAL OVERVIEW—DRUG DEMAND, DRUG SUPPLY. In *World Drug Report 2022*; United Nations Office on Drugs and Crime (Ed.) United Nations Publication: Vienna, Austria, 2022; Volume Booklet 2, pp. 1–83, ISBN 9789211483758.
3. United Nations Office on Drugs and Crime. (Ed.) United Nations Office on Drugs and Crime Drug Market Trends: Cocaine, Amphetamine-Type Stimulants, New Psychoactive Substances. In *World Drug Report 2022*; United Nations publication: Vienna, Austria, 2022; Volume Booklet 4, pp. 1–111, ISBN 9789211483758.

4. Couto, R.A.S.; Gonçalves, L.M.; Carvalho, F.; Rodrigues, J.A.; Rodrigues, C.M.P.; Quinaz, M.B. The Analytical Challenge in the Determination of Cathinones, Key-Players in the Worldwide Phenomenon of Novel Psychoactive Substances. *Crit. Rev. Anal. Chem.* **2018**, *48*, 372–390. [CrossRef] [PubMed]

5. Custódio, M.F.; Magalhães, L.O.; Arantes, L.C.; Braga, J.W.B. Identification of Synthetic Drugs on Seized Blotter Papers Using ATR-FTIR and PLS-DA: Routine Application in a Forensic Laboratory. *J. Braz. Chem. Soc.* **2021**, *32*, 513–522. [CrossRef]

6. Skoog, D.A.; Holler, F.J.; Nieman, T.A. *Princípios de Análise Instrumental*, 5th ed.; Bookman: Porto Alegre, Brazil, 2002; ISBN 85-7307-976-2.

7. Rohman, A.; Windarsih, A.; Hossain, M.A.M.; Johan, M.R.; Ali, M.E.; Fadzilah, N.A. Application of Near- and Mid-Infrared Spectroscopy Combined with Chemometrics for Discrimination and Authentication of Herbal Products: A Review. *J. Appl. Pharm. Sci.* **2019**, *9*, 137–147. [CrossRef]

8. Manley, M.; Baeten, V. Spectroscopic Technique: Near Infrared (NIR) Spectroscopy. In *Modern Techniques for Food Authentication*; Elsevier: Amsterdam, The Netherlands, 2018; pp. 51–102.

9. Beć, K.B.; Grabska, J.; Huck, C.W. NIR Spectroscopy of Natural Medicines Supported by Novel Instrumentation and Methods for Data Analysis and Interpretation. *J. Pharm. Biomed. Anal.* **2021**, *193*, 113686. [CrossRef]

10. Pavia, D.L.; Lampman, G.M.; Kriz, G.S.; Vyvyan, J.A. *Introduction to Spectroscopy*, 4th ed.; Cengage Learning: Boston, MA, USA, 2008; ISBN1 10: 0-495-11478-2; ISBN2 13: 978-0-495-11478-9.

11. Levine, I.N. *Quantum Chemistry*; Pearson Prentice Hall: Upper Saddle River, NJ, USA, 2009; p. 751.

12. Ning, Y.-C. (Ed.) Yong-Cheng Ning Interpretation of Infrared Spectra. In *Interpretation of Organic Spectra*; Wiley: Hoboken, NJ, USA, 2011; pp. 129–146.

13. Coates, J. Interpretation of Infrared Spectra, A Practical Approach. In *Encyclopedia of Analytical Chemistry*; John Wiley & Sons, Ltd.: Chichester, UK, 2006.

14. Scientific Working Group for the Analysis of Seized Drugs, (SWGDRUG). *SWGDRUG Recommendations Version 7.1*; United States Department of Justice: Washington, DC, USA, 2016.

15. Magalhães, D.F.; Santos, F.J.V.; Barbosa, D.M.D. Aplicações Da Espectroscopia de Infravermelho Próximo Na Monitorização de Processos Farmacêuticos. Master's Thesis, Faculdade de Ciências da Universidade de Lisboa: Lisboa, Portugal, 2014.

16. Kranenburg, R.F.; Weesepoel, Y.; Alewijn, M.; Sap, S.; Arisz, P.W.F.; van Esch, A.; Keizers, P.H.J.; van Asten, A.C. Dataset of Near-Infrared Spectral Data of Illicit-Drugs and Forensic Casework Samples Analyzed by Five Portable Spectrometers Operating in Different Wavelength Ranges. *Data Brief* **2022**, *45*, 108660. [CrossRef]

17. Kranenburg, R.F.; Weesepoel, Y.; Alewijn, M.; Sap, S.; Arisz, P.W.F.; van Esch, A.; Keizers, P.H.J.; van Asten, A.C. The Importance of Wavelength Selection in On-Scene Identification of Drugs of Abuse with Portable Near-Infrared Spectroscopy. *Forensic Chem.* **2022**, *30*, 100437. [CrossRef]

18. Kranenburg, R.F.; Ou, F.; Sevo, P.; Petruzzella, M.; de Ridder, R.; van Klinken, A.; Hakkel, K.D.; van Elst, D.M.J.; van Veldhoven, R.; Pagliano, F.; et al. On-Site Illicit-Drug Detection with an Integrated Near-Infrared Spectral Sensor: A Proof of Concept. *Talanta* **2022**, *245*, 123441. [CrossRef]

19. Kranenburg, R.F.; Ramaker, H.; Sap, S.; van Asten, A.C. A Calibration Friendly Approach to Identify Drugs of Abuse Mixtures with a Portable Near-infrared Analyzer. *Drug Test Anal.* **2022**, *14*, 1089–1101. [CrossRef]

20. Alonzo, M.; Alder, R.; Clancy, L.; Fu, S. Portable Testing Techniques for the Analysis of Drug Materials. *WIREs Forensic Sci.* **2022**, *4*, e1461.

21. Kranenburg, R.F.; Ramaker, H.-J.; van Asten, A.C. Portable near Infrared Spectroscopy for the Isomeric Differentiation of New Psychoactive Substances. *Forensic Sci. Int.* **2022**, *341*, 111467. [CrossRef] [PubMed]

22. Trinklein, T.J.; Thapa, M.; Lanphere, L.A.; Frost, J.A.; Koresch, S.M.; Aldstadt, J.H. Sequential Injection Analysis Coupled to On-Line Benchtop Proton NMR: Method Development and Application to the Determination of Synthetic Cathinones in Seized Drug Samples. *Talanta* **2021**, *231*, 122355. [CrossRef] [PubMed]

23. Zhao, Y.; Wu, B.; Hua, Z.; Xu, P.; Xu, H.; Shen, W.; Di, B.; Wang, Y.; Su, M. Quantification of Cathinone Analogues without Reference Standard Using 1H Quantitative NMR. *Anal. Sci.* **2021**, *37*, 1577–1582. [CrossRef] [PubMed]

24. Groombridge, C.J. NMR Spectroscopy in Forensic Science. In *Annual Reports on NMR Spectroscopy*; Academic Press: Cambridge, MA, USA, 1996; pp. 215–297.

25. Hulme, M.C.; Hayatbakhsh, A.; Brignall, R.M.; Gilbert, N.; Costello, A.; Schofield, C.J.; Williamson, D.C.; Kemsley, E.K.; Sutcliffe, O.B.; Mewis, R.E. Detection, Discrimination and Quantification of Amphetamine, Cathinone and *nor*-ephedrine Regioisomers Using Benchtop ^{1}H and [19]F Nuclear Magnetic Resonance Spectroscopy. *Magn. Reson. Chem.* **2021**. mrc.5156, *early view*. [CrossRef]

26. Seibert, E.; Kunert, O.; Pferschy-Wenzig, E.-M.; Schmid, M.G. Characterization of Three Novel 4-Methylaminorex Derivatives Applied as Designer Drugs. *Molecules* **2022**, *27*, 5770. [CrossRef]

27. Kranenburg, R.F.; Stuyver, L.I.; de Ridder, R.; van Beek, A.; Colmsee, E.; van Asten, A.C. Deliberate Evasion of Narcotic Legislation: Trends Visualized in Commercial Mixtures of New Psychoactive Substances Analyzed by GC-Solid Deposition-FTIR. *Forensic Chem.* **2021**, *25*, 100346. [CrossRef]

28. Laposchan, S.; Kranenburg, R.F.; van Asten, A.C. Impurities, Adulterants and Cutting Agents in Cocaine as Potential Candidates for Retrospective Mining of GC-MS Data. *Sci. Justice* **2022**, *62*, 60–75. [CrossRef]

29. Md Ghazi, M.G.; Lee, L.C.; Sino, H.; Abdul Halim, M.I. Review of Contemporary Chemometric Strategies Applied on Preparing GC–MS Data in Forensic Analysis. *Microchem. J.* **2022**, *181*, 107732. [CrossRef]

30. Boronat Ena, M.D.M.; Cowan, D.A.; Abbate, V. Ambient Ionization Mass Spectrometry Applied to New Psychoactive Substance Analysis. *Mass Spectrom. Rev.* **2021**, *42*, mas.21695. [CrossRef]

31. Waldman, W.; Kała, M.; Lechowicz, W.; Gil, D.; Anand, J.S. Severe Clinical Toxicity Caused by 25I-NBOMe Confirmed Analytically Using LC-MS-MS Method. *Acta Biochim. Pol.* **2018**, *65*, 567–571. [CrossRef]

32. Fogarty, M.F.; Papsun, D.M.; Logan, B.K. Analysis of Fentanyl and 18 Novel Fentanyl Analogs and Metabolites by LC-MS-MS, and Report of Fatalities Associated with Methoxyacetylfentanyl and Cyclopropylfentanyl. *J. Anal. Toxicol.* **2018**, *42*, 592–604. [CrossRef]

33. Ferreira, M.M.C. *QUIMIOMETRIA—Conceitos, Métodos e Aplicações*, 1st ed.; Editora da Unicamp: Campinas, Brazil, 2015.

34. Roux, C.; Bucht, R.; Crispino, F.; de Forest, P.; Lennard, C.; Margot, P.; Miranda, M.D.; NicDaeid, N.; Ribaux, O.; Ross, A.; et al. The Sydney Declaration—Revisiting the Essence of Forensic Science through Its Fundamental Principles. *Forensic Sci. Int.* **2022**, *332*, 111182. [CrossRef] [PubMed]

35. Mistek-Morabito, E.; Lednev, I.K. Discrimination of Menstrual and Peripheral Blood Traces Using Attenuated Total Reflection Fourier Transform-Infrared (ATR FT-IR) Spectroscopy and Chemometrics for Forensic Purposes. *Anal. Bioanal. Chem.* **2021**, *413*, 2513–2522. [CrossRef] [PubMed]

36. Sharma, S.; Kaur, H.; Singh, R. Sex Discrimination from Urine Traces for Forensic Purposes Using Attenuated Total Reflectance Fourier Transform Infrared Spectroscopy and Multivariate Data Analysis. *Int. J. Leg. Med.* **2022**, *136*, 1755–1765. [CrossRef] [PubMed]

37. Newland, T.G.; Pitts, K.; Lewis, S.W. Multimodal Spectroscopy with Chemometrics for the Forensic Analysis of Western Australian Sandy Soils. *Forensic Chem.* **2022**, *28*, 100412. [CrossRef]

38. Takamura, A.; Ozawa, T. Recent Advances of Vibrational Spectroscopy and Chemometrics for Forensic Biological Analysis. *Analyst* **2021**, *146*, 7431–7449. [CrossRef] [PubMed]

39. Aljannahi, A.; Alblooshi, R.A.; Alremeithi, R.H.; Karamitsos, I.; Ahli, N.A.; Askar, A.M.; Albastaki, I.M.; Ahli, M.M.; Modak, S. Forensic Analysis of Textile Synthetic Fibers Using a FT-IR Spectroscopy Approach. *Molecules* **2022**, *27*, 4281. [CrossRef] [PubMed]

40. Qiu, W.; Li, W. Non-Destructive Characterization and Discrimination of Vehicle Bumpers Fragments in Forensic Science Using Molecular Spectral Fusion Analysis and Chemometrics. *Microchem. J.* **2021**, *167*, 106299. [CrossRef]

41. Sauzier, G.; van Bronswijk, W.; Lewis, S.W. Chemometrics in Forensic Science: Approaches and Applications. *Analyst* **2021**, *146*, 2415–2448. [CrossRef]

42. Popovic, A.; Morelato, M.; Roux, C.; Beavis, A. Review of the Most Common Chemometric Techniques in Illicit Drug Profiling. *Forensic Sci. Int.* **2019**, *302*, 109911. [CrossRef]

43. Risoluti, R.; Materazzi, S.; Gregori, A.; Ripani, L. Early Detection of Emerging Street Drugs by near Infrared Spectroscopy and Chemometrics. *Talanta* **2016**, *153*, 407–413. [CrossRef] [PubMed]

44. Salonen, T.; Ahrens, B.; Bovens, M.; Eliaerts, J.; Huhtala, S.; Nordgaard, A.; Alberink, I. Chemometrics in Forensic Chemistry—Part II: Standardized Applications—Three Examples Involving Illicit Drugs. *Forensic Sci. Int.* **2020**, *307*, 110138. [CrossRef] [PubMed]

45. Bruni, A.T.; de Carvalho, P.O.M.; Rodrigues, C.H.P.; Leite, V.B.P. *In silico* Methods in Forensic Science: Quantum Chemistry and Multivariate Analysis Applied to Infrared Spectra of New Amphetamine- and Cathinone-Derived Psychoactive Substances. *Forensic Chem.* **2018**, *9*, 21–34. [CrossRef]

46. Braz, A.; Santos Silva, C.; Peixoto, A.C.; Pimentel, M.F.; Pereira, G.; Caixeta Castro Souza Braga, P.; Martini, A.L.; Lino Fernandes Alcântara, T. Preliminary Study on the Identification of Synthetic Cathinones in Street Seized Samples by Raman Spectroscopy and Chemometrics. *J. Raman Spectrosc.* **2021**, *52*, 901–913. [CrossRef]

47. Tcharkhetian, A.E.G.; Bruni, A.T.; Rodrigues, C.H.P. Combining Experimental and Theoretical Approaches to Study the Structural and Spectroscopic Properties of Flakka (α-Pyrrolidinopentiophenone). *Results Chem.* **2021**, *3*, 100254. [CrossRef]

48. Rodrigues, C.H.P.; Leite, V.B.P.; Bruni, A.T. Can NMR Spectroscopy Discriminate between NPS Amphetamines and Cathinones? An Evaluation by in silico Studies and Chemometrics. *Chemom. Intell. Lab. Syst.* **2021**, *210*, 104265. [CrossRef]

49. De Santana, D.C.A.S.; de Santana, F.J.M. A Brief Overview on the Importance of Analyzing Drug Adulterants in the Treatment of Non-Fatal Overdose and Substance Use Disorder of Street Cocaine. *Forensic Toxicol.* **2021**, *39*, 275–281. [CrossRef]

50. Dragan, A.-M.; Parrilla, M.; Feier, B.; Oprean, R.; Cristea, C.; de Wael, K. Analytical Techniques for the Detection of Amphetamine-Type Substances in Different Matrices: A Comprehensive Review. *TrAC Trends Anal. Chem.* **2021**, *145*, 116447. [CrossRef]

51. Campos, E.; de Martinis, E.; de Martinis, B. Forensic Analysis of Illicit Drugs and Novel Psychoactive Substances in Wastewater: A Review of Toxicological, Chemical and Microbiological Aspects. *Braz. J. Anal. Chem.* **2021**, *9*, 15–34. [CrossRef]

52. Harper, L.; Powell, J.; Pijl, E.M. An Overview of Forensic Drug Testing Methods and Their Suitability for Harm Reduction Point-of-Care Services. *Harm Reduct. J.* **2017**, *14*, 52.

53. Arsić, B.; Lukić, V.; Micić, R.; Radosavljević, Ž.; Nedović, B. Overview of the Major Classes of New Psychoactive Substances, Psychoactive Effects, Analytical Determination and Conformational Analysis of Selected Illegal Drugs. *Open Chem.* **2021**, *19*, 60–106.

54. Goncalves, R.; Titier, K.; Latour, V.; Peyré, A.; Castaing, N.; Daveluy, A.; Molimard, M. Suitability of Infrared Spectroscopy for Drug Checking in Harm Reduction Centres. *Int. J. Drug Policy* **2021**, *88*, 103037. [PubMed]

55. Bunaciu, A.A.; Aboul-Enein, H.Y. Adulterated Drug Analysis Using FTIR Spectroscopy. *Appl. Spectrosc. Rev.* **2021**, *56*, 423–437. [CrossRef]

56. Andreasen, M.F.; Lindholst, C.; Kaa, E. Adulterants and Diluents in Heroin, Amphetamine, and Cocaine Found on the Illicit Drug Market in Aarhus, Denmark. *Open Forensic Sci. J.* **2009**, *2*, 16–20. [CrossRef]

57. Becke, A.D. Density-functional Thermochemistry. III. The Role of Exact Exchange. *J. Chem. Phys.* **1993**, *98*, 5648–5652. [CrossRef]

58. Lee, C.; Yang, W.; Parr, R.G. Development of the Colle-Salvetti Correlation-Energy Formula into a Functional of the Electron Density. *Phys. Rev. B* **1988**, *37*, 785–789. [CrossRef]

59. Schäfer, A.; Huber, C.; Ahlrichs, R. Fully Optimized Contracted Gaussian Basis Sets of Triple Zeta Valence Quality for Atoms Li to Kr. *J. Chem. Phys.* **1994**, *100*, 5829–5835. [CrossRef]

60. Weigend, F.; Ahlrichs, R. Balanced Basis Sets of Split Valence, Triple Zeta Valence and Quadruple Zeta Valence Quality for H to Rn: Design and Assessment of Accuracy. *Phys. Chem. Chem. Phys.* **2005**, *7*, 3297. [CrossRef]

61. Schäfer, A.; Horn, H.; Ahlrichs, R. Fully Optimized Contracted Gaussian Basis Sets for Atoms Li to Kr. *J. Chem. Phys.* **1992**, *97*, 2571–2577. [CrossRef]

62. Neese, F. Software Update: The ORCA Program System, Version 4.0. *WIREs Comput. Mol. Sci.* **2018**, *8*, 73–78. [CrossRef]

63. Barone, V.; Cossi, M. Quantum Calculation of Molecular Energies and Energy Gradients in Solution by a Conductor Solvent Model. *J. Phys. Chem. A* **1998**, *102*, 1995–2001. [CrossRef]

64. Takano, Y.; Houk, K.N. Benchmarking the Conductor-like Polarizable Continuum Model (CPCM) for Aqueous Solvation Free Energies of Neutral and Ionic Organic Molecules. *J. Chem. Theory Comput.* **2005**, *1*, 70–77. [PubMed]

65. Johnson, R. NIST 101. Computational Chemistry Comparison and Benchmark Database, CCCBDBDComputational Chemistry Comparison and Benchmark Database, [online]. 1999. Available online: http://cccbdb.nist.gov (accessed on 17 February 2022).

66. Saccenti, E.; Hendriks, M.H.W.B.; Smilde, A.K. Corruption of the Pearson Correlation Coefficient by Measurement Error and Its Estimation, Bias, and Correction under Different Error Models. *Sci. Rep.* **2020**, *10*, 438. [CrossRef] [PubMed]

67. Webb, G.I.; Sammut, C.; Perlich, C.; Horváth, T.; Wrobel, S.; Korb, K.B.; Noble, W.S.; Leslie, C.; Lagoudakis, M.G.; Quadrianto, N.; et al. Leave-One-Out Cross-Validation. In *Encyclopedia of Machine Learning*; Springer: Boston, MA, USA, 2011; pp. 600–601.

68. Szymańska, E.; Saccenti, E.; Smilde, A.K.; Westerhuis, J.A. Double-Check: Validation of Diagnostic Statistics for PLS-DA Models in Metabolomics Studies. *Metabolomics* **2012**, *8*, 3–16. [CrossRef] [PubMed]

69. Wold, S.; Sjöström, M.; Eriksson, L. PLS-Regression: A Basic Tool of Chemometrics. *Chemom. Intell. Lab. Syst.* **2001**, *58*, 109–130. [CrossRef]

70. De Melo, E.; Martins, J.; Rodrigues, C.; Bruni, A. *In silico* Risk Assessment Studies of New Psychoactive Substances Derived from Amphetamines and Cathinones. *J. Braz. Chem. Soc.* **2020**, *31*, 927–940. [CrossRef]

71. Kennard, R.W.; Stone, L.A. Computer Aided Design of Experiments. *Technometrics* **1969**, *11*, 137. [CrossRef]

72. Amin, M.O.; Al-Hetlani, E.; Lednev, I.K. Detection and Identification of Drug Traces in Latent Fingermarks Using Raman Spectroscopy. *Sci. Rep.* **2022**, *12*, 3136. [CrossRef]

73. Fernandes, D.D.D.S. Novas Estratégias Para Seleção de Variáveis Por Intervalos Em Problemas de Classificação. Ph.D Thesis, Universidade Federal da Paraíba: João Pessoa, Brazil, 2016.

74. Santana, F.; Souza, A.; Almeida, M.; Breitkreitz, M.; Filgueiras, P.; Sena, M.; Poppi, R. Experimento didático de quimiometria para classificação de óleos vegetais comestíveis por espectroscopia no infravermelho médio combinado com análise discriminante por mínimos quadrados parciais: Um tutorial, parte V. *Quim Nova* **2020**, *43*, 371–381. [CrossRef]

75. Youden, W.J. Index for Rating Diagnostic Tests. *Cancer* **1950**, *3*, 32–35. [CrossRef]

76. López, M.I.; Callao, M.P.; Ruisánchez, I. A Tutorial on the Validation of Qualitative Methods: From the Univariate to the Multivariate Approach. *Anal. Chim. Acta* **2015**, *891*, 62–72. [CrossRef]

77. Scientific Working Group for the Analysis of Seized Drugs (SWGDRUG); Center for Forensic Science Research and Education (CFSRE). Forensic Drug Review; KGI School of Pharmacy and Health Sciences N-Ethylpentylone. *Monographs SWGDRUG* **2016**, 1–5. Available online: https://www.swgdrug.org/Monographs/N-Ethylpentylone.pdf (accessed on 15 November 2021).

78. Amin, M.O.; Al-Hetlani, E.; Lednev, I.K. Trends in Vibrational Spectroscopy of Fingermarks for Forensic Purposes. *TrAC Trends Anal. Chem.* **2021**, *143*, 116341. [CrossRef]

79. Chen, Y.; Wen, D.; Pei, J.; Fei, Y.; Ouyang, D.; Zhang, H.; Luo, Y. Identification and Quantification of Microplastics Using Fourier-Transform Infrared Spectroscopy: Current Status and Future Prospects. *Curr. Opin. Env. Sci. Health* **2020**, *18*, 14–19. [CrossRef]

80. Noda, I. Two-Trace Two-Dimensional (2T2D) Correlation Spectroscopy—A Method for Extracting Useful Information from a Pair of Spectra. *J. Mol. Struct.* **2018**, *1160*, 471–478. [CrossRef]

81. Özer, Z.; Kılıç, T.; Çarıkçı, S.; Azizoglu, A. Synthesis, Structural Characterization, Spectroscopic Properties, and Theoretical Investigation of Siderol Acetate. *Russ. J. Phys. Chem. A* **2019**, *93*, 2703–2709. [CrossRef]

82. Laury, M.L.; Carlson, M.J.; Wilson, A.K. Vibrational Frequency Scale Factors for Density Functional Theory and the Polarization Consistent Basis Sets. *J. Comput. Chem.* **2012**, *33*, 2380–2387. [CrossRef]

83. De Castro, J.S.; Rodrigues, C.H.P.; Bruni, A.T. *In silico* Infrared Characterization of Synthetic Cannabinoids by Quantum Chemistry and Chemometrics. *J. Chem. Inf. Model.* **2020**, *60*, 2100–2114. [CrossRef]

84. Costa, A.S.; Martins, J.P.A.; de Melo, E.B. SMILES-Based 2D-QSAR and Similarity Search for Identification of Potential New Scaffolds for Development of SARS-CoV-2 MPRO Inhibitors. *Struct. Chem.* **2022**, *33*, 1691–1706. [CrossRef]

85. Kiralj, R.; Ferreira, M.M.C. Basic Validation Procedures for Regression Models in QSAR and QSPR Studies: Theory and Application. *J. Braz. Chem. Soc.* **2009**, *20*, 770–787. [CrossRef]

86. Lavine, B.; Almirall, J.; Muehlethaler, C.; Neumann, C.; Workman, J. Criteria for Comparing Infrared Spectra—A Review of the Forensic and Analytical Chemistry Literature. *Forensic Chem.* **2020**, *18*, 100224. [CrossRef]

87. Cole, C.; Jones, L.; McVeigh, J.; Kicman, A.; Syed, Q.; Bellis, M. Adulterants in Illicit Drugs: A Review of Empirical Evidence. *Drug Test Anal.* **2011**, *3*, 89–96. [CrossRef] [PubMed]

88. Fiorentin, T.R.; Logan, B.K.; Martin, D.M.; Browne, T.; Rieders, E.F. Assessment of a Portable Quadrupole-Based Gas Chromatography Mass Spectrometry for Seized Drug Analysis. *Forensic Sci. Int.* **2020**, *313*, 110342. [CrossRef] [PubMed]

89. Dixon, D.I.; Antonides, L.H.; Costello, A.; Crane, B.; Embleton, A.; Fletcher, M.L.; Gilbert, N.; Hulme, M.C.; James, M.J.; Lever, M.A.; et al. Comparative Study of the Analysis of Seized Samples by GC-MS, 1H NMR and FT-IR Spectroscopy within a Night-Time Economy (NTE) Setting. *J. Pharm. Biomed. Anal.* **2022**, *219*, 114950. [CrossRef] [PubMed]

90. Fregonese, M.; Albino, A.; Covino, C.; Gili, A.; Bacci, M.; Nicoletti, A.; Gambelunghe, C. Drug Checking as Strategy for Harm Reduction in Recreational Contests: Evaluation of Two Different Drug Analysis Methodologies. *Front. Psychiatry* **2021**, *12*, 596895. [CrossRef]

91. Davidson, J.T.; Lum, B.J.; Nano, G.; Jackson, G.P. Comparison of Measured and Recommended Acceptance Criteria for the Analysis of Seized Drugs Using Gas Chromatography–Mass Spectrometry (GC–MS). *Forensic Chem.* **2018**, *10*, 15–26. [CrossRef]

92. Wallace, B.; Hills, R.; Rothwell, J.; Kumar, D.; Garber, I.; Roode, T.; Larnder, A.; Pagan, F.; Aasen, J.; Weatherston, J.; et al. Implementing an Integrated Multi-technology Platform for Drug Checking: Social, Scientific, and Technological Considerations. *Drug Test Anal.* **2021**, *13*, 734–746. [CrossRef]

93. Green, T.C.; Park, J.N.; Gilbert, M.; McKenzie, M.; Struth, E.; Lucas, R.; Clarke, W.; Sherman, S.G. An Assessment of the Limits of Detection, Sensitivity and Specificity of Three Devices for Public Health-Based Drug Checking of Fentanyl in Street-Acquired Samples. *Int. J. Drug Policy* **2020**, *77*, 102661. [CrossRef]

94. Moore, J.M.; Casale, J.F.; Klein, R.F.X.; Cooper, D.A.; Lydon, J. Determination and In-Depth Chromatographic Analyses of Alkaloids in South American and Greenhouse-Cultivated Coca Leaves. *J. Chromatogr. A* **1994**, *659*, 163–175. [CrossRef]

95. Ribaux, O.; Baylon, A.; Roux, C.; Delémont, O.; Lock, E.; Zingg, C.; Margot, P. Intelligence-Led Crime Scene Processing. Part I: Forensic Intelligence. *Forensic Sci. Int.* **2010**, *195*, 10–16. [CrossRef]

96. Ribaux, O.; Girod, A.; Walsh, S.J.; Margot, P.; Mizrahi, S. Forensic Intelligence and Crime Analysis. *Law Probab. Risk* **2003**, *2*, 47–60. [CrossRef]

97. Ribaux, O.; Talbot Wright, B. Expanding Forensic Science through Forensic Intelligence. *Sci. Justice* **2014**, *54*, 494–501. [CrossRef] [PubMed]

98. Esseiva, P.; Ioset, S.; Anglada, F.; Gasté, L.; Ribaux, O.; Margot, P.; Gallusser, A.; Biedermann, A.; Specht, Y.; Ottinger, E. Forensic Drug Intelligence: An Important Tool in Law Enforcement. *Forensic Sci. Int.* **2007**, *167*, 247–254. [CrossRef] [PubMed]

99. Houhou, R.; Bocklitz, T. Trends in Artificial Intelligence, Machine Learning, and Chemometrics Applied to Chemical Data. *Anal. Sci. Adv.* **2021**, *2*, 128–141.

100. Baechler, S.; Morelato, M.; Gittelson, S.; Walsh, S.; Margot, P.; Roux, C.; Ribaux, O. Breaking the Barriers between Intelligence, Investigation and Evaluation: A Continuous Approach to Define the Contribution and Scope of Forensic Science. *Forensic Sci. Int.* **2020**, *309*, 110213. [CrossRef]

101. Morelato, M.; Baechler, S.; Ribaux, O.; Beavis, A.; Tahtouh, M.; Kirkbride, P.; Roux, C.; Margot, P. Forensic Intelligence Framework—Part I: Induction of a Transversal Model by Comparing Illicit Drugs and False Identity Documents Monitoring. *Forensic Sci. Int.* **2014**, *236*, 181–190. [CrossRef]

102. Pereira, L.S.A.; Lisboa, F.L.C.; Coelho Neto, J.; Valladão, F.N.; Sena, M.M. Screening Method for Rapid Classification of Psychoactive Substances in Illicit Tablets Using Mid Infrared Spectroscopy and PLS-DA. *Forensic Sci. Int.* **2018**, *288*, 227–235. [CrossRef]